RSC Advances

ROYAL SOCIETY OF CHEMISTRY

www.rsc.org/advances

Journal Name

ARTICLE

Implications for blood-brain-barrier permeability, *in vitro* oxidative stress and neurotoxicity potential induced by mesoporous silica nanoparticles: effects of surface modification

Received 00th January 20xx,
Accepted 00th January 20xx

DOI: 10.1039/x0xx00000x

www.rsc.org/

Ming Zhou‡,[a] Linlin Xie‡,[a] Chen-Jie Fang,*[a] Hua Yang,[b] Yan-Jie Wang,[c] Xiao-Yu Zhen,[c] Chun-Hua Yan,*[c] Yuji Wang,[a] Ming Zhao*[a,d] and Shiqi Peng*[a]

Increasing in abundance and practical applications of nanomaterials has led to growing concern over the potential adverse effects of the nanoparticles on human health. The unique structure makes mesoporous silica nanoparticles (MSNs) an ideal platform for developing multifunctional nanocarriers, including non-viral gene delivery in the central nerve system (CNS). However, the potential neurotoxicity of the MSNs remains largely unclear. In this study, we explored the bio-effect of MCM-41 type MSNs on blood-brain-barrier (BBB) permeability, neuronal damage, and mediation of neurotoxicity with surface chemistry. With or without a ligand transferrin (Tf) which could interact with transferrin receptor expressed at the BBB, *in vivo* imaging indicated that both MSN–Cy–Tf and MSN–Cy may enter into the brain, suggesting the potential to deliver the therapeutic agents across the BBB. However, risk arises associated with this permeability. Histological observation of the hippocampus confirms the CNS devliery of MSNs and indicates the neuronal damage, characterized by neuronal cell loss, nuclei shrinkage, and disintegration of neurons, reminiscent of *in vivo* neurotoxicity. With PC12 cell, a paradigm for dopaminergic neuron, *in vitro* examination suggests that various surface modified MSNs decrease the cell viability and caused oxidative stress with elevation of reactive oxygen spices (ROS), depletion of glutathione (GSH), leakage of lactate dehydrogenase (LDH), and generation of malondialdehyde (MDA) in a concentration-dependent manner. Compared with the pristine MSNs which induce the severest injury impacts on the cells, thiol modified MSN–SH nanoparticle shows significantly slight injury effects among the test MSNs, suggesting the possibility to mediate the neurotoxicity via the surface chemistry to modify this kind of the nanomaterials in the biomedical applications.

1. Introduction

Blood-brain-barrier (BBB) represents the strictest biological barrier to protect the brain. For more than 98% drugs treating central nervous system (CNS) disorders, however, this barrier is also a formidable obstacle for the effective delivery of the therapeutic agents to the brain. Therefore, there is a clear need for various strategies to deliver nonpermeating CNS therapeutic agents crossing BBB.[1, 2] Within the boosting nanomaterials, nanoparticles would be an efficient alternative for brain drug delivery. However the interactions of nanomaterials with various biological systems and barriers, especially BBB, as well as the toxic/bio effect of nanomaterials are still largely unknown.[3] Up to date, only limited works show that the deposition of the nanomaterials in the brain can cause oxidative stress, tissue damage, and neurotoxicity,[4, 5] whereas precise pathway of neuron damage and mechanism remains principally unclear.

Brain tissue is mainly composed of neuron and glial cells. As core cells neurons are critical for brain function. The neuronal damage, including defect of structure and/or loss of function, plays a crucial role in the aging and some neurodegenerative diseases, such as Parkinson's diseases and Alzheimer's diseases. Due to large amount of oxygen consume and oxidant production whilst antioxidant deficiency, the brain and CNS are particularly susceptible to oxidative stress induced by reactive oxygen species (ROS).[6, 7] The oxidants derived from ROS like H_2O_2 and $OH^{\cdot -}$ are highly reactive toward DNA, proteins, and lipids, causing significant destruction to the cells.[8, 9] As an essential physiological regulator, ROS normally exists in cells in a balance with antioxidant.[10] The excessive oxidants will induce lipid peroxidation, DNA damage, and tissue toxicity.[11]

[a] *Beijing area major laboratory of peptide and small molecular drugs; Engineering Research Center of Endogenous Prophylactic of Ministry of Education of China; Beijing Laboratory of Biomedical Materials; College of Pharmaceutical Sciences, Capital Medical University, Beijing 100069, P.R. China. Email:sqpeng@ccmu.edu.cn*
[b] *Medical Experimental & Test Centre, Capital Medical University, Beijing 100069, China.*
[c] *Beijing National Laboratory for Molecular Sciences, State Key Laboratory of Rare Earth Materials Chemistry and Applications & PKU-HKU Joint Laboratory on Rare Earth Materials and Bioinorganic Chemistry, Peking University, Beijing 100871, China.*
[d] *Faculty of Biomedical Science and Environmental Biology, Kaohsiung Medical University, Kaohsiung, Taiwan*
Electronic Supplementary Information (ESI) available: [Additional materials characterization technique (Figure S1). Images of the deep brain slices (Figure S2). Correlation plot of the levels of ROS, GSH, and MDA versus the level of LDH for various MSNs]. See DOI: 10.1039/x0xx00000x. See DOI: 10.1039/x0xx00000x
‡These authors contributed equally to this work.

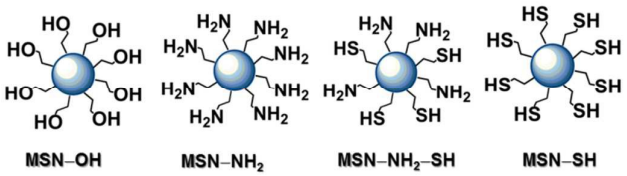

Chart 1 MSNs with only silanol residue (MSN–OH) and surface modified MSN–NH_2, MSN–NH_2–SH, and MSN–SH.

Since Mobil researchers reported synthesis of mesoporous silica,[12] burgeoning area of porous silica research, especially mesoporous silica nanoparticles (MSNs), has been their use as nanocarriers in applications of therapy and diagnosis.[13, 14] MSNs possess unique structural characters such as large surface area, tunable pore size and channel, and well-defined surface property, which make MSNs an ideal platform for drug delivery[15-19] and further lead to substantial research regarding their chemical stability, biodistribution and excretion, biocompatibility and biosafety.[16, 20-22] While the beneficial aspects are widely publicized, some new concerns including the negative impact of the MSNs on living cells and tissue have arisen. It is still unknown such as whether the MSNs could enter the brain and exert adverse effects, and how the MSNs interact with the brain tissues and neurons.

Although toxicity of silicon and silica has been continually studied for more than a century,[23-30], little is known about possible adverse effects on the brain once silica enter the CNS. As silica nanoparticles (SiNPs) are generally deemed nontoxic, SiNPs have been formulated for non-viral gene delivery in the CNS.[31, 32] However, Guilarte *et al*. first examined the effects of SiNPs (150 to 200 nm) exposure on the brain using primary rat microglia.[33] The results suggested that very low levels of SiNPs increase the ROS production and are capable of altering microglial function. Wu *et al*. demonstrated that SiNPs (15 nm) possibly have a negative impact on the striatum and dopaminergic neurons as well a potential risk for neurodegenerative diseases.[34] To the best of our knowledge, so far no study has been carried out to define the effects of the MSNs on BBB permeability, neuron damage and oxidative stress. Because high surface-to-volume ratio of nanomaterials could create more potential for enhanced cellular interactions and different pathways of toxicity compared with coarse grained silica,[26, 35-37] it is urgent to explore the (neuro)toxicity of ordered MSNs and the relationship with nanoparticles' physicochemical property.[26, 38-40] In this context, we explored the *in vivo* BBB permeability, neuron damage, and *in vitro* oxidative stress induced by the MSNs with different surface groups (Chart 1).

2. Experimental section

2.1 Synthesis and characterization of the MSNs

MSN–NH_2, MSN–NH_2–SH, and MSN–SH were synthesized by co-condensation method according to our previous work.[41, 42] For MSN–Cy, fluorescent dye Cy5.5 was attached covalently to MSN–NH_2 via amide bonds. Then, transferrin (Tf) was attached covalently to MSN–Cy at room temperature in dark overnight to fabricate MSN–Cy–Tf. The nanoparticles were collected by centrifugation, and the supernatant were collected for analysis. Particles were then washed and sonicated several times in order to remove any adsorbed protein and then dried in vacuum.

Power X-ray diffraction (XRD) patterns of the nanoparticles were recorded on Rigaku D/Max-2000 X-ray powder diffractometer (Japan) using Cu K_α (λ = 1.5405 Å) radiation. TEM images were taken on the JEM-2100 transmission electron microscope under a working voltage of 200 kV. The nitrogen adsorption and desorption isotherms were measured on an ASAP 2010 analyser (Micromeritics Co. Ltd.) at 78 K. The surface charge of the nanoparticles was measured with Zetasizer (NanoZS Malvern Inst., Malvern, UK). Size distribution was also measured using dynamic light scattering (DLS) with the Zetasizer.

2.2 *In vivo* animal studies

The animal studies were approved by the Animal Ethical Committee of Capital Medical University (China). Six-week-old male nude mice were purchased from Weitonglihua Laboratory Animal Co., Ltd. (Beijing, China). Six mice per cage were housed under standard laboratory conditions (12 h light : 12 h dark and 24 ± 3°C), rodent diet and water were provided ad libitum. The experiments were initiated one week after arrival of the animals.

2.2.1 *In vivo* imaging. Fluorescence from Cy5.5 attached on MSN–Cy and MSN–Cy–Tf in mice was obtained using NightOWL LB983 *in vivo* imaging system (Berthold Technologies, Germany, excitation: 635–675 nm, emission: 695–740 nm), which is equipped with cooled backside illuminated NightOWL II CCD camera, along with image acquisition and analysis software (IndiGO software). The fluorescence intensity of MSN–Cy and MSN–Cy–Tf was height-corrected.

2.2.2 Hematoxylin and eosin (H&E) staining. After exposure to MSN–Cy and MSN–Cy–Tf for 0.5 h, the mice were sacrificed by decapitation and their brains were dissected and immersed in 4% paraformaldehyde, fixed at 4°C for at least 24 h, and then processed by routine histological methods. The coronary slices (5μm) were obtained and used for hematoxylin and eosin (H&E) staining in accordance with the standard procedure. The eosin imparts a pink to red color to cytoplasm, and the hematoxylin stains nucleus blue. The slices were observed on an Olympus SZX-MDHSW microscope (Japan) and photographed.

2.3 *In vitro* studies

2.3.1 Cell culture and differentiation. PC12 cell line was obtained from the Beijing Xiehe Cell Bank of Type Culture Collection. The cells were grown in RPMI 1640 medium (Hyclone, USA) containing 5% fetal bovine serum (FBS), 100 U mL^{-1} penicillin, 100 μg mL^{-1} streptomycin, 10% horse serum, and 50 ng ml^{-1} nerve growth factor at 37°C in an atmosphere of 5% CO_2.

The stock solution of the MSNs was prepared serially from 1 to 200 μg mL^{-1} of the samples. These samples were sonicated before exposure to the mice and cells to produce a less-aggregated and uniform suspension. For the *in vitro* experiments, the freshly dispersed MSNs suspensions were immediately applied to the cells. The cells free of the MSNs were used as the control.

2.3.2 MTT assay. The cytotoxicity of the MSNs was evaluated with standard MTT (3-(4,5-dimethylthiazol-2-yl)-2,5-diphenyl-2H-tetrazolium bromide) assay. Briefly, PC12 cells were planted in 96-well plates (Corning, Inc., New York, USA) at a density of 2×10^4 cells per well in growth medium RPMI 1640. After 24 h incubation, the MSNs of various concentrations were loaded into the 96-well plates, and the viability of PC12 cells was determined. 100 μL of MTT was added into each well and incubated for 4 h till purple crystals to be visible. After removal of MTT solution, the purple formazan crystals were dissolved in 100 μL of DMSO and the absorbance was measured at 490 nm on a microplate reader (BIO-RAD Model1680, USA). The cytotoxicity was expressed as % of inhibition rate.

2.3.3 Intracellular ROS determination. DCFH-DA is a membrane-permeant compound and, once inside the cells, it is deacetylated by endogenous esterases to form the nonfluorescent 2',7'-dichlorfluorescein (DCFH). DCFH is converted to fluorescent dichlorofluorescein (DCF) by cellular oxidation. As a result, green fluorescence emits in response to ROS production and can be analyzed by flow cytometry. Briefly, DCFH-DA (Sigma) was re-suspended in DMSO. The cells were incubated with DCFH-DA solution at a final concentration of 10 μM in RPMI 1640 without serum for 30 min at 37°C in 5% CO_2 atmosphere. Afterward, the cells were rinsed twice with PBS and centrifuged, and then the supernatant was discarded to collect the pellets. The pellets were resuspended in PBS, and the data were collected by using the Becton-Dickinson FACS Aria flow cytometer ($\lambda_{Ex}/\lambda_{Em}$ = 488/525 nm) and analyzed with BD-FACS Diva 4.1 software. ROS level was expressed as the ratio of the mean intensity of the treated group versus mean intensity of the control group.

2.3.4 Intracellular glutathione (GSH) measurement. The intracellular GSH content was measured with a glutathione assay kit (Sigma-Aldrich, USA). Briefly, PC12 cells were plated in six-well plates at a density of 5.0×10^5 cells per well and treated with various suspensions of the MSNs. After 24 h treatment, the cells were first deproteinized with 5% 5-sulfosalicylic acid, centrifuged to remove the precipitated protein, and then the intracellular GSH content was measured according to the manufacturer's instructions. The absorbance at 412 nm was measured with microreader (BIO-RAD Model1680, USA). GSH level was expressed as the ratio of the mean intensity of the treated group versus the mean intensity of the control group.

2.3.5 Malondialdehyde (MDA) measurement. After exposure to the MSNs for 24 h, the cells were scraped off, collected, rinsed with PBS to remove culture medium, and then resuspended in 0.5% cold Triton X-100. Cell lysates were centrifuged to remove debris, and the supernatants were used for intracellular MDA assays. MDA content was measured with MDA kit (Jiancheng, Nanjing, China) according to the manufacturer's instructions. The absorbance at 530 was measured with microreader (BIO-RAD Model1680, USA). The MDA concentration (nmol mg^{-1}protein) in the samples was extrapolated from the standard curve. Results were represented as % change in MDA concentration as compared to the control.

2.3.6 Lactate dehydrogenase (LDH) measurement. LDH leakage is based on the activity measurement of cytoplasmic enzyme LDH in the extracellular space. At the end of 24 h exposure to the MSNs, the culture medium was centrifuged and the cell-free supernatant was collected. The activity of LDH in the medium was determined with a commercial LDH kit (Jiancheng, Nanjing, China) according to the manufacturer's protocol. The absorption was measured with a microreader (BIO-RAD Model1680, USA) at 440 nm, and LDH levels in the medium versus the cells were quantified and compared to the control.

2.3.7 Statistical analysis. The results are represented as mean ± standard deviation (SD) (*n* equals at least 3) and were further analysed by one-way analysis of variance (ANOVA). The comparisons are considered to be significantly different from each other when a *p* value is smaller than 0.05 and highly significantly different when *p* value smaller than 0.01.

3. Results

3.1 Characterization of MSNs

The surface modified MSNs were prepared by co-condensation of functional trimethoxysilane and tetraethyl orthosilicate, and were characterized with typical techniques. The powder X-ray diffraction (XRD, Fig. S1) patterns of the MSNs with different surface groups show a typical two-dimensional hexagonal p_6mm mesophase and display expected features of MCM-41 type mesoporous structure, with the main peaks indexed to (100) diffraction of a hexagonal structure. Fig. 1 indicates that all the MSNs show highly ordered hexagonally arranged mesopores with one-dimensional channels throughout the particles. Combination of X-ray patterns and TEM images demonstrates that the surface functionalization of the MSNs remains the mesoporous structure of MCM-41 type silica. Generally, the silica nanoparticles tend to aggregate, due to H-bonding interactions between residual silanol groups. This nature has to be reduced in the biological applications, in

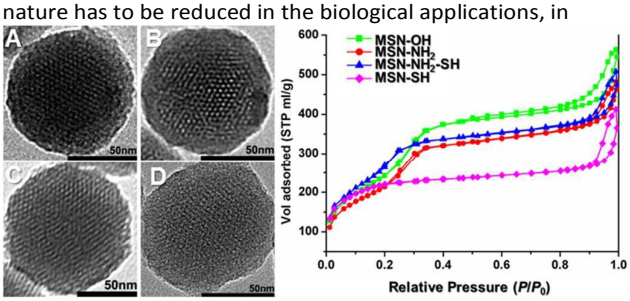

Fig. 1 (Left) Transmission electron microscopy (TEM) of the nanoparticles of MSN–OH (A), MSN–NH_2 (B), MSN–NH_2–SH(C), and MSN–SH (D). (Right) BET N_2 adsorption-desorption isotherms of MSN–OH, MSN–NH_2, MSN–NH_2–SH, and MSN–SH at 78K.

Table 1 The physicochemical data of functionalized MSNs

MSNs	Radius (nm)	ξ (mV)	Surface area (m^2g^{-1})	Pore diameter (nm)
MSN–OH	278.5±8.62	–8.75±3.03	843.17	3.34
MSN–NH_2	266.1±12.0	2.30±0.12	745.31	3.28
MSN–NH_2–SH	271.5±0.42	0.30±0.06	918.31	2.70
MSN–SH	247.4±1.63	3.09±0.25	764.74	2.39

* The zeta-potential ξ was measured in PBS (0.067 M, pH = 7.4)

order to improve cellular uptake, biodistribution, and biocompatibility, etc. Though surface modification does not change the mesophase structure of MCM-41, it indeed mediates the surface property of MCM-41, which was examined with nitrogen adsorption and desorption isotherms at 78K. The surface properties of the modified MSNs are shown in Fig.1 and listed in Table 1. Compared with pristine MSN–OH (mean radius: 3.34 nm), thiol-modified MSN–SH has the lowest adsorption capacity and the slimmest channel (mean radius: 2.39 nm). During the fabrication, the functional groups may interact with the micelles upon formation and thus result in a reduction in pore size and shrinkage of unit cell size. The physicochemical data in Table 1 indicate that the particle size of all modified MSNs ranges in 200 to 300 nm, and zeta-potential changes dramatically with the groups conjugated on the surface of the MSNs. The zeta-potential are –8.75 ± 3.03, 2.30 ± 0.12, 0.30 ± 0.06 and 3.09 ± 0.25 mV for MSN–OH, MSN–NH_2, MSN–NH_2–SH, and MSN–SH, respectively. When ligand Tf was conjugated with the MSNs, the value for MSN–Cy–Tf is –6.71 ± 3.03 mV, compared to 35.01 ± 2.12 mV for MSN–Cy.

3.2 BBB permeable potential of the MSNs

The BBB prevent from entering of exogenous species from blood into brain and maintains brain homeostasis.[43] The BBB permeability and brain accumulation of MSN–Cy–Tf and MSN–Cy were examined with *in vivo* fluorescent imaging (Fig. 2) and further confirmed with tissue sectioning method (Figs. S2). *In vivo* fluorescent images were taken at designed time intervals after tail intravenous injection. Surprisingly, the fluorescence of both MSN–Cy–Tf and MSN–Cy was obviously observed in the brain of treated mice after injection only 1 min, indicating that both MSN–Cy–Tf and MSN–Cy could enter the brain very quickly (Fig. 2). The accumulation of MSN–Cy in the brain at designed intervals is comparable to that of MSN–Cy–

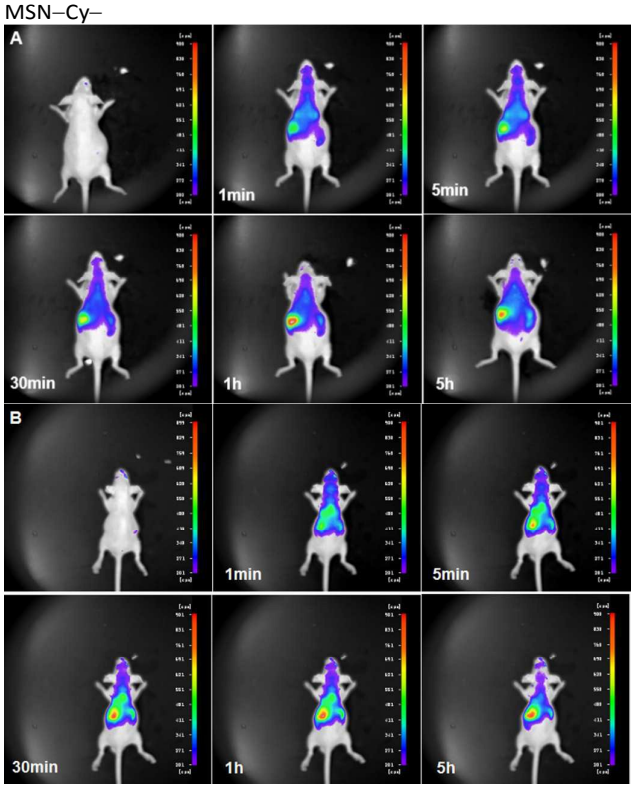

Fig. 2 Distribution of MSNs in nude mice after tail intravenous administration at a dose of 0.1 mL/10g (v/body weight). The MSNs were dispersed in 5% glucose to prepare 1 mg/mL injection. Images were taken at designed interval time after administration. (A) Image of MSN–Cy treated mouse; (B) Image of MSN–Cy–Tf treated mouse.

Tf, indicating that effect of the ligand Tf on the kinetics of the MSNs across the BBB is slight. The concentration of the MSNs gradually decreased several minutes after injection. In addition, the accumulation of the MSNs is also remarkable in the peripheral tissues such as kidneys, liver, and spleen. The fluorescence intensity in these tissues implies that the concentration and kinetics of accumulation in the liver, kidney, and spleen may be higher and faster than that in the brain. Nevertheless, more extensive studies are needed to confirm the permeability and kinetics of the MSNs across the BBB and to reveal the mechanism of the MSNs entering the brain.

3.3 Histological observation of hippocampus

In order to further validity the permeability of the MSNs, we selected hippocampus in the brain as a specific target to observe the effect of the MSNs exposure on neuronal

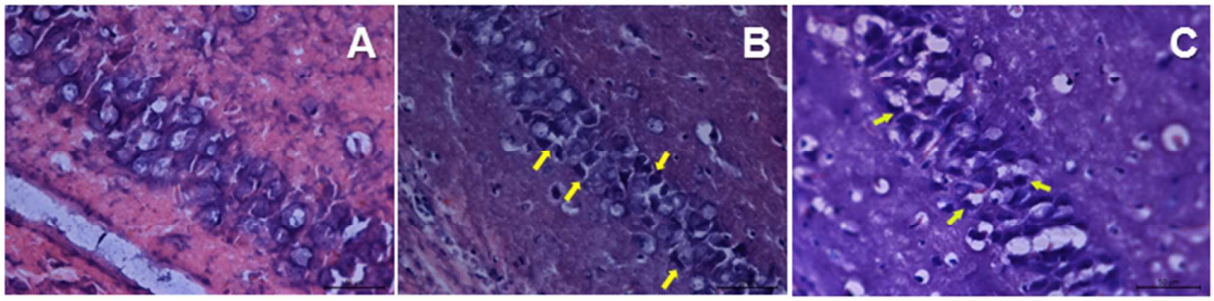

Fig.3 Neuropathological changes in hippocampus stained with H&E. (A) Hippocampus of untreated mice (control); (B) Hippocampus of MSN–Cy–Tf treated mice; (C) Hippocampus of MSN–Cy treated mice. The mice were sacrificed 30 min after injection. The arrows show the dead neuron cells. The scale bar is 50 μm.

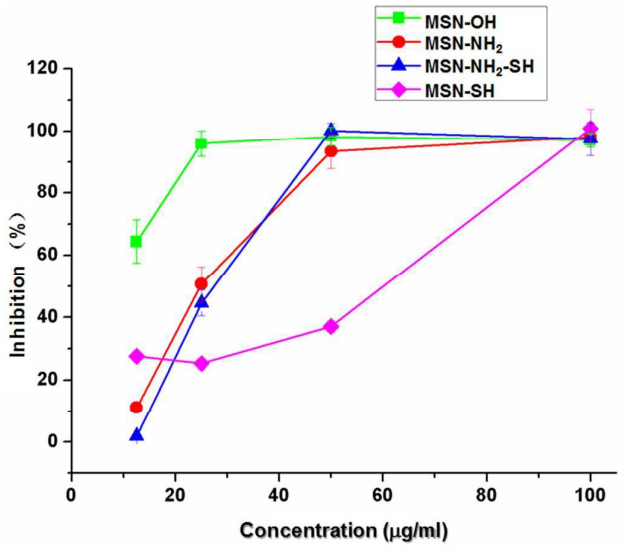

Fig. 4 The concentration dependent cytotoxicity induced by–OH, –NH_2, –NH_2–SH, and –SH modified MSNs. Inhibition rate of various MSNs to PC12 cell was determined with MTT assay after 24 h exposure. Cells cultured in medium without MSNs are control. Data are represented with mean ± SD (n = 3).

morphological changes by H&E staining. For this purpose, the mice were sacrificed 30 min after injection, taking into account the concentration of the MSNs retaining in the brain and the time allowed for the interaction between the MSNs and the tissues. And then the brain was excised and subjected to sectioning and staining. The representative images are illustrated in Fig.3. In control group, round and dark stained neurons arranged approximately layer by layer and packed regularly with the chromatin of the nucleus being stained homogeneously. The neuronal morphological changes in the hippocampus are clear in the MSN–Cy and MSN–Cy–Tf treated groups. The exposure of MSN–Cy and MSN–Cy–Tf evoked a discernible alteration in the hippocampus, which was characterized by neuronal loss and thinning of cell layers, nuclei shrinkage, and disintegration and dark staining of neurons. For the MSN–Cy treated mice, more vacuoles appeared in the hippocampus, compared with that of MSN–Cy–Tf treated mice. The results of the present study suggest the potential that the MSNs go across the BBB, accumulate in the brain, and damage the neurons of the hippocampus.

3.4 *In vitro* cytotoxicity of various surface modified MSNs

To explore the *in vitro* cytotoxicity of the MSNs, we examined the proliferation of the MSNs treated PC12 cells, a paradigm for neurobiological studies, with MTT assay.[44] In brief, PC12 cells were exposed to the modified MSNs at 12.5 μg mL^{-1} to 100 μg mL^{-1} for 24 h. As shown in Fig. 4. the inhibition percentage of MSN–OH, MSN–NH_2 and MSN–NH_2–SH reaches the maximum at 50 μg mL^{-1}, while that of MSN–SH reaches the maximum at 100 μg mL^{-1}. The IC_{50} values (50% inhibitory concentration) of 24 h exposure are 5.8, 26.9, 27.1, and 48.7 μg mL^{-1} for MSN–OH, MSN–NH_2, MSN–NH_2–SH, and MSN–SH, respectively, suggesting that the pristine MSN–OH shows the highest cytotoxicity.

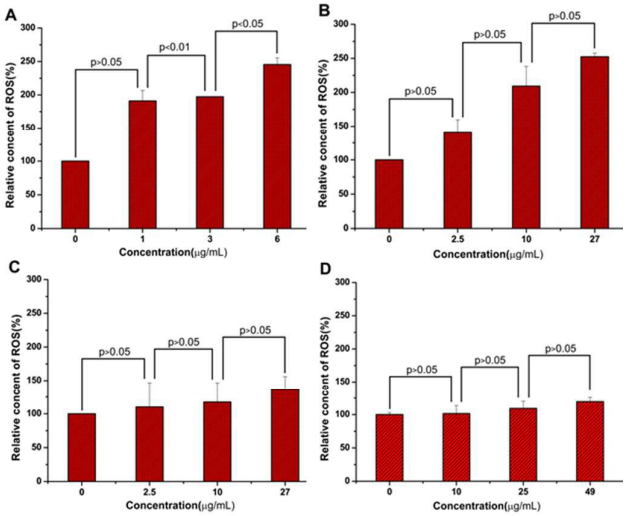

Fig. 5 Effect of the MSNs on ROS elevation. PC12 cells without the MSNs are the control. The PC12 cells were cultured with various concentrations of the MSNs (A: MSN–OH, B: MSN–NH_2, C: MSN–NH_2–SH, and D: MSN–SH) for 24 h. Intracellular ROS elevation is surface- and concentration-dependent. Data are represented with mean ± SD (n = 3).

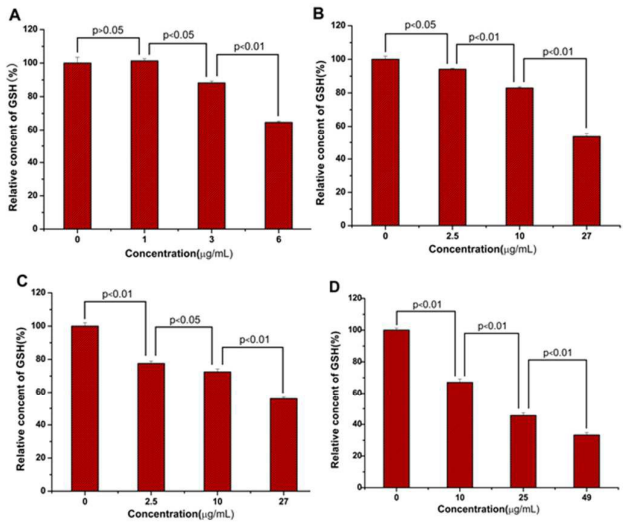

Fig. 6 Effect of the MSNs on GSH reduction. PC12 cells without the MSNs are the control. The PC12 cells were cultured with various concentrations of the MSNs (A: MSN–OH, B: MSN–NH_2, C: MSN–NH_2–SH, and D: MSN–SH) for 24 h. Intracellular GSH reduction is surface- and concentration-dependent. Data are represented with mean ± SD (n = 3).

3.5 Molecular mechanism of MSNs damaging neurons

To reveal the molecular mechanism of neuronal damage induced by the MSNs, we measured the levels of ROS, GSH, LDH, and MDA in the MSNs treated PC12 cells.

3.5.1 ROS elevation of MSNs treated PC12 cells. ROS is a collective term of free oxygen radicals, such as superoxide anion, hydroxyl radicals, hydrogen peroxide and ozone. ROS are involved in pathogenesis of a variety of inflammatory conditions, and the increase of intracellular ROS level causes the damage of cell structure and eventually results in cell death or apoptosis.[45] The oxidative stress of PC12 cells induced by the MSNs was assessed with measuring the intracellular ROS level, which was quantified with DCFH-DA method.[46] The result (Fig. 5) suggests that the ROS elevation induced by the MSNs is surface- and concentration- dependent. MSN–OH and MSN–NH_2 treated cells have the highest ROS level, which are 2.5-fold higher than that of the control group. However, the ROS level of the MSN–NH_2–SH and MSN–SH treated cells equal that of the control cells. It is also found that, at IC_{50} concentration, 6 μg mL^{-1} MSN–OH and 27 μg mL^{-1} MSN–NH_2 caused 2.5-fold increase of intracellular ROS, 27 μg mL^{-1} MSN–NH_2–SH caused 1.4-fold increase of ROS, and 49 μg mL^{-1} MSN–SH caused only 1.1-fold increase of ROS. The result implies that the surface effect on the ROS generation is different for various surface modified MSNs.

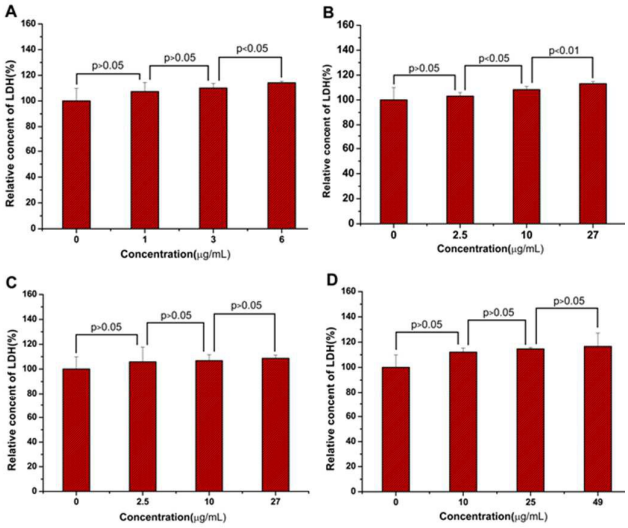

Fig.7 Effect of the MSNs on LDH leakage. PC12 cells without the MSNs are the control. PC12 cells were cultured with various concentrations of the MSNs (A: MSN–OH, B: MSN–NH_2, C: MSN–NH_2–SH, and D: MSN–SH) for 24 h. The extracellular LDH content is surface-and concentration-dependent. Data are represented with mean ± SD (n = 3).

3.5. 2 GSH depletion. GSH is a key antioxidant in the body and plays crucial roles in maintaining the homeostasis of cellular oxidation-reduction. Alteration in GSH homeostasis can be considered as an indication of functional damage of the cells, due that excessive radicals can give rise to lipid peroxidation and cell membrane damage. As shown in Fig. 6, the effect of the MSNs on intracellular GSH depletion depends on the concentration and surface group. Relative to the control, 64.6%, 48.0%, 55.9% and 33.2% of intracellular GSH were remained for MSN–OH at 6 μg mL^{-1}, MSN–NH_2 at 27 μg mL^{-1} MSN–NH_2–SH at 27 μg mL^{-1}, and MSN–SH at 49 μg mL^{-1}, respectively.

3.5.3 LDH leakage. LDH is an enzyme widely present in cytosol that can convert lactate to pyruvate. It will be released into the culture media when the biomembrane integrity is altered or disrupted. The extracellular LDH level depends on the material/chemical toxicity, and it is a reflective of cell membrane integrity. The effects of surfaces of the MSNs on LDH leakage are shown in Fig. 7. The different surface modified MSNs do not alter the leakage of LDH significantly.

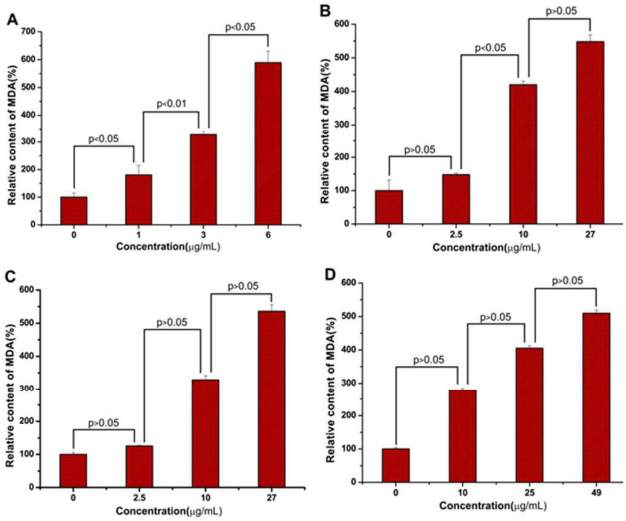

Fig.8 Effect of the MSNs on MDA production. PC12 cells without the MSNs are the control. PC12 cells were cultured with various concentrations of the MSNs (A: MSN–OH, B: MSN–NH_2, C: MSN–NH_2–SH, and D: MSN–SH) for 24 h. MDA production is surface- and concentration-dependent. Data are represented with mean ± SD (n = 3).

3.5.4 MDA generation. MDA is an end product of lipid peroxidation and serves as a reliable detection index of lipid peroxidation. The results of the present study (Fig. 8) imply that the MSNs may induce oxidative damage to PC12 cells. All the MSNs show a concentration- and surface- dependent effect on MDA generation. Overall, the generation of MDA of all the MSNs treated PC12 cells is 4 to 5 folds higher than that of the control group. For every kind of MSNs, the generation of MDA is at the same level in PC12 cells treated at various concentrations of MSNs, e. g. 6 μg mL^{-1} of MSN–OH, 27 μg mL^{-1} of MSN–NH_2, 27 μg mL^{-1} of MSN–NH_2–SH, and 49 μg mL^{-1} of MSN–SH. It indicated that the surface effect is different for the MDA generation.

4. Discussion

Developing CNS drug delivery to go across the BBB is a challenging but meaningful task.[47, 48] Over past few years, the nanoparticles have shown the potential to overcome the BBB and transport the therapeutic agents into the brain via intravenous administration. And yet a majority of these nanoparticles have focused on primarily colloid carriers such as liposomes, polymeric nanoparticles, solid lipid nanoparticles, polymeric micelles, and dendrimers.[49-52] The most accepted mechanism for the brain uptake of these nanoparticles

appears to be transcytosis mediated by specific receptors expressed at the BBB, such as lipoprotein, transferrin receptor and insulin receptor.[51, 53] In our present work, in vivo imaging indicates that even the MSNs without Tf modification may go across the BBB and enter the brain.

The mechanism of the nanoparticles across the BBB depends on the materials' structural and physicochemical properties, such as particle size, charge/surface potential, H-bonding potential, and lipophilicity, etc.[54] Most of the successful exemplary nanoparticles used to deliver various drug into the brain ranged in the size from 150 to 300 nm, which may affect the endocytic uptake mechanism.[55] Surface charge and hydrophobicity also influence the uptake. Generally, non-ionic and hydrophobic surfaces are rapidly opsonized followed by recognition by the reticular endothelial system, and higher internalization rates are usually associated with positively charged particles because of the negatively charged component of the cell membranes.[56, 57] However, negatively charged nanoparticles can also yield efficient uptake, especially after adsorption or covalently coupling of targeting ligands.[58] MSN–Cy–Tf (253.6 ± 7.50 nm) and MSN–Cy (257.1 ± 2.97 nm) used in this study have −6.71 ± 3.03 mV and 35.01 ± 2.12 mV of zeta-potential, respectively. It seems that both zeta-potential and particle size influence the uptake of the nanoparticles.[59-61] Further study is needed to elucidate the mechanism of the nanoparticles entering the brain.

Risks rise associated with the MSNs entering in the brain. Therefore, it is meaningful to demonstrate the possibility of the accumulation of the MSNs in the brain. Herein we performed a histopathological observation of the hippocampus, a typical tissue of the brain and a critical integration centre for cognitive functions such as learning and memory. ROS can trigger deleterious effects in the brain[62, 63] because excessive ROS could result in lipid peroxidation in the hippocampus, striatum, and frontal cortex, etc.[64, 65] The hippocampus is particularly sensitive to lipid peroxidation due to high level of polyunsaturated fatty acids and iron,[63] both of which are the target of free radicals. In addition, the hippocampus possesses low level of antioxidants.[66] As the cell at the portal-of-entry sites in the brain, the neuronal response to the MSNs exposure was morphologically examined. The morphological changes, such as neuronal nuclear shrinkage, vacuole appearance and necrotic neurons in the hippocampus indicate the risks of the neuronal damage and neurotoxicity of MSN–Cy and MSN–Cy–Tf treatment. In respect of neuronal damage, the damage by MSN–Cy is severer than that by MSN–Cy–Tf, might due to more positive surface charge and therefore stronger interaction of MSN–Cy with the negatively charged cell membrane.[56, 57, 67]

The most discussed paradigm for the toxicity of the nanomaterials is oxidative stress,[68-73] attributed to ROS elevation. Some *in vivo* studies have demonstrated that the nanomaterials can escape from the BBB and accumulate in the brain cause CNS damage, in which oxidative stress are vital and important.[74, 75] It has been well-established that ROS production and oxidative stress play a crucial role as the important mechanisms involved in the health effects of both micro- and nano-sized silicon and silica, whatever crystalline or amorphous materials.[26, 76-81] Generally, prime toxicity of the silica materials is attributed to surface radicals ($SiO^{\bullet}$, $SiO_2^{\bullet}$, $SiO_3^{\bullet}$ and $Si{+}O_2^{\bullet-}$), which can react with water to yield ROS, and thus result in oxidative stress to damage DNA and proteins[8, 34, 82, 83] and then affect cell cycle progression via initiating apoptosis. In addition, through H-bonding and electrostatic interactions with the biomembrane components the MSNs can cause toxic reaction.[84] In this study, we used PC12 cells to investigate the potential neurotoxicity of the MSNs and to explain the mechanisms of neurotoxicity by correlating the surface modification with oxidative stress indicated by the levels of ROS, GSH, LDH, and MDA.

Table 2 R^2 of correlation between LDH level and ROS, GSH, and MDA levels, respectively

Samples	ROS versus LDH	GSH versus LDH	MDA versus LDH
MSN–OH	0.9078	0.9973	0.9973
MSN–NH_2	0.9883	0.9252	0.9676
MSN–NH_2–SH	0.9946	0.9855	0.9719
MSN–SH	0.9803	0.9922	0.9999

The MTT assay of PC12 cells exposed in MSN–OH, MSN–NH_2, MSN–NH_2–SH, and MSN–SH for 24 h addressed a concentration-dependent toxicity. MSN–OH, MSN–NH_2, and MSN–NH_2–SH show severe cytotoxicity at 50 μg mL^{-1}, with the inhibition higher than 90%. Though MSN–SH at 12.5 μg mL^{-1} shows high inhibition, it shows the lowest inhibition among the test MSNs at 25 ~ 50 μg mL^{-1}. Of four kinds of the MSNs, MSN–OH shows the severest cytotoxicity whereas MSN–SH shows the slightest cytotoxicity, as indicated by the IC_{50} value, which of MSN–OH is 7-fold lower than that of MSN–SH. Since the size and shape of the MSNs used in this work are identical, the effect of the size and shape on the cytotoxicity is ignorable. In respect of surface charge and hydroxyl coverage, MSN–OH has the profoundest negative potential and the largest hydroxyl coverage. In addition to the intrinsically presence of surface radicals and ROS generation, the H-bonding and electrostatic interactions of the MSNs with the biomembrane should also contribute to the cytotoxicity. In contrast, MSN–SH could provide the reductive thiol to alleviate the oxidative stress and damage, giving rise to the slightest cytotoxicity.

It is known that many intracellular redox processes are driven by redox property of thiol group, and intracellular protection against oxidation can be mediated by thiol–disulfide exchange between inflow thiol and oxidized glutathione.[85, 86] After MSN–SH is internalized by PC12 cells, the radicals $SiO^{\bullet}$, $SiO_2^{\bullet}$, $SiO_3^{\bullet}$ and $Si{+}O_2^{\bullet-}$ from silica surface could generate reactive $HO^{\bullet}$ radical and induce oxidative stress. When GSSG(glutathione disulfide)/GSH ratio rises, the depletion of GSH could be prevented by the thiol of MSN–SH, giving rise to regeneration of GSH through exchange the thiol of MSN–SH with GSSG. The highest IC_{50} and the slightest oxidative stress of MSN–SH treated PC12 cells suggest that MSN–SH is able to reduce GSSG to GSH through a

nonenzymatic thiol–disulfide exchange and protect the cells from the oxidative stress thereby alleviate the neurotoxicity.

To correlate the cytotoxicity with oxidative stress, we examined oxidative stress biomarkers, LDH, ROS, MDA, and GSH. LDH level in the media can be an indicator of cytotoxicity, because damage to the biomembranes can trigger release of intracellular LDH, which induces a chain reaction of further cell death.[87] It was found that cytotoxicity indicated by LDH level and oxidative stress indexed by ROS, MDA, and GSH are linearly correlated to each other (Fig. S3). In the most cases the correlation coefficient R^2 is larger than 0.95 (Table 2), suggesting that the cytotoxicity appears strongly relevant to oxidative stress manifested by elevated ROS, depleted GSH, and increased MDA. The elevation of ROS seems to deplete cellular GSH significantly, induce lipid peroxidation, produce MDA, alter the biomembrane integrity, result in LDH leakage, and eventually lead to cell death. The excessive ROS in PC12 cells directly oxidizes the DNA, proteins, and lipids, thereby damages the biomembranes and its functions, consequently associates with the activation of apoptosis.[8, 63] It is known that apoptosis can be triggered at the mitochondria, cell membrane receptors and chromosomal DNA.[88] MTT and LDH measurements in this work suggest mitochondrial injury, which may be produced by oxidative stress. In response to these death stimuli, the mitochondria may initiate programmed cell death and apoptosis.[89, 90]

Conclusions

In summary, we performed the *in vivo* imaging experiment to examine the potential of the MSNs across the BBB with or without the ligand Tf and direct biological effects of the MSNs on PC12 cells, and further the neurotoxicity of the MSNs was also explored. The *in vivo* results suggest that the MSNs may go across the BBB, accumulate in the brain, and induce the hippocampal neuronal damage. *In vitro* exposure of the MSNs resulted in cellular morphological changes and oxidative stress, as indicated by elevation of intracellular ROS which triggered cell death in a concentration-dependent manner, as well GSH depletion, MDA generation, and LDH leakage. The fitting of oxidative stress to the cytotoxicity caused by the various MSNs correlate the surface chemistry with oxidative stress and thus neurotoxicity. Further studies are needed to address the mechanism of the internalization and oxidative stress to reveal the basis of the neurotoxicity induced by the MSNs. The present study sheds light on the possibility to mediate the neurotoxicity via the surface modification of the MSNs in biomedical applications.

Acknowledgements

The authors thank the NSFC (21171120, 21571133), Natural Science Foundation of Beijing Municipality (7132020), Beijing Municipal Science & Technology Commission (Z141100002114049), and TJSHG (201310025008) for financial support.

Notes and references

1. P. Blasi, S. Giovagnoli, A. Schoubben, M. Ricci and C. Rossi, *Adv. Drug Deliv. Rev.*, 2007, **38**, 454-477.
2. W. M. Pardridge, *Curr Opin Pharmacol*, 2006, **6**, 494–500.
3. G. K. Wolfgang, S. B. Manuela, T. Shinji and M. Winfried, *Acc. Chem. Res.*, 2013, **43**.
4. T. R. Pisanic, *Biomaterials*, 2007, **28**, 2572-2581.
5. S. M. Hussain, *Toxicol. Sci.*, 2006, **92**, 456-463.
6. E. Gitto, R. J. Reiter, M. Karbownik, D. Tan, P. Gitto, S. Barberi and I. Barberi, *Biol. Neonate.* , 2002, **81**, 146-157.
7. R. Piga, *Neurotoxicology*, 2007, **28**, 67-75.
8. J. F. Turrens, *J. Physiol.*, 2003, **552**, 335–344.
9. K. J. Barnham and C. L. Masters, *Nat. Rev. Drug Discovery*, 2004, **3**, 205-214.
10. A. A. C. Suzy and C. E. Serpil, *Am. J. Physiol.-Lung. C.* , 2002, **283**, 246-255.
11. D. Trachootham, J. Alexandre and P. Huang, *Nat. Rev. Drug Discov.* , 2009, **8**, 579-591.
12. J. S. Beck, J. C. Vartuli, W. J. Roth, M. E. Leonowicz, C. T. Kresge, K. D. Schmitt, C. T. W. Chu, D. H. Olson and E. W. Sheppard, *J. Am. Chem. Soc.*, 1992, **114**, 10834-10843.
13. B. G. Trewyn, I. I. Slowing, S. Giri, H. T. Chen and V. S. Y. Lin, *Acc. Chem. Res.*, 2007, **40**, 846-853.
14. Z. Tao, *RSC Advances*, 2014, **4**, 18961.
15. M. Vallet-Regi, F. Balas and D. Arcos, *Angew.Chem. Int. Ed.*, 2007, **46**, 7548-7558.
16. J. E. Lee, N. Lee, T. Kim, J. Kim and T. Hyeon, *Acc. Chem. Res.*, 2011, **44**, 893-902.
17. M. W. Ambrogio, C. R. Thomas, Y.-L. Zhao, J. I. Zink and J. F. Stoddart, *Acc. Chem. Res.*, 2011, **44**, 903-913.
18. I. I. Slowing, J. L. Vivero-Escoto, C.-W. Wu and V. S.-Y. Lin, *Adv. Drug Deliv. Rev.*, 2008, **60**, 1278-1288.
19. Q. He and J. Shi, *Adv. Mater.*, 2014, **26**, 391-411.
20. D. Tarn, C. E. Ashley, M. Xue, E. C. Carnes, J. I. Zink and C. J. Brinker, *Acc. Chem. Res.*, 2013, **46**, 792-801.
21. A. Popat, S. B. Hartono, F. Stahr, J. Liu, S. Z. Qiao and Q. L. Gao, *Nanoscale*, 2011, **3**, 2801.
22. J. M. Rosenholm, C. Sahlgren and M. Lindén, *Nanoscale*, 2010, **2**, 1870-1883.
23. V. Castranova and V. Vallyathan, *Environ. Health. Persp.*, 2000, **108 suppl 4**, 3-14.
24. K. Donaldson and P. J. A. Borm, *Ann. Occup. Hyg.*, 1998, **42**, 287–294.
25. B. Rimal, *Curr. Opin. Pulm.Med.*, 2005, **11**, 169-173.
26. D. Napierska, L. C. J. Thomassen, D. Lison, J. A. Martens and P. H. Hoet, *Part. Fibre. Toxicol.* , 2010, **7**, 39.
27. V. Castranova, V. Vallyathan and W. E. Wallace, *Silica and silica-induced lung diseases*, CRC Press, 1996.
28. G. M. Calvert, F. L. Rice, J. M. Boiano, J. W. Sheehy and W. T. Sanderson, *Occup. Environ. Med*, 2003, **60**, : 122–129.
29. D. D. Dunnom, *Health effects of synthetic silica particulates : a symposium*, American Society for Testing and Materials, 1981.
30. J. K. Mclaughlin, W. H. Chow and L. S. Levy, *J. Toxico. Environ. Health*, 1997, **50**, 553-566.
31. I. Roy, T. Y. Ohulchanskyy, D. J. Bharali, H. E. Pudavar, R. A. Mistretta, N. Kaur and P. N. Prasad, *Proc. Natl. Acad. Sci. USA*, 2005, **102**, 279-284.
32. D. J. Bharali, I. Klejbor, E. K. Stachowiak, P. Dutta, I. Roy, N. Kaur, E. J. Bergey, P. N. Prasad and M. K. Stachowiak, *Proc. Natl. Acad. Sci. USA*, 2005, **102**, 11539-11544.

33. J. Choi, Q. Zheng, H. E. Katz and T. R. Guilarte, *Environ. Health. Persp.*, 2010, **118**, 589-595.
34. J. Wu, C. Wang, J. Sun and Y. Xue, *ACS Nano*, 2011, **5**, 4476-4489.
35. H. Meng, M. Xue, T. Xia, Z. Ji, D. Y. Tarn, J. I. Zink and A. Nel, *ACS Nano*, 2011, , 4131-4144.
36. G. Oberdörster, E. Oberdörster and J. Oberdörster, *Environ. Health. Persp.* , 2005, **113**, 823-839.
37. S. K. Natarajan and S. Selvaraj, *RSC Advances*, 2014, **4**, 14328.
38. I. Fenoglio, G. Martra, S. Coluccia and B. Fubini, *Chem. Res. Toxicol.*, 2000, **13**, 971-975.
39. K. M. Waters, L. M. Masiello, R. C. Zangar, B. J. Tarasevich, N. J. Karin, R. D. Quesenberry, S. Bandyopadhyay, J. G. Teeguarden, J. G. Pounds and B. D. Thrall, *Toxicol. Sci.* , 2009, **107**, 553-569.
40. C. Minjung, C. Wan-Seob, C. Mina, J. K. Sueng, S. H. Beom, H. K. Sheen, O. K. Hyoung, Y. S. Yhun and J. Jayoung, *Toxicol. Lett.*, 2009, **189**, 177–183.
41. R. Guo, L. L. Li, W. H. Zhao, Y. X. Chen, X. Z. Wang, C. J. Fang, W. Feng, T. L. Zhang, X. Ma, M. Lu, S. Q. Peng and C. H. Yan, *Nanoscale*, 2012, **4**, 3577-3583.
42. W. Wang, C. Fang, X. Wang, Y. Chen, Y. Wang, W. Feng, C. Yan, M. Zhao and S. Peng, *Nanoscale*, 2013, **5**, 6249-6253.
43. N. J. Abbott, A. A. Patabendige, D. E. Dolman, S. R. Yusof and D. J. Begley, *Neurobiol. Dis.*, 2010, **37**, 13–25.
44. T. Ishima, T. Nishimura, M. Iyo and K. Hashimoto, *Prog. Neuropsychopharmacol. Biol. Psychiatry.*, 2008, **32**, 1656-1659.
45. M. Ott, V. Gogvadze, S. Orrenius and B. Zhivotovsky, *Apoptosis*, 2007, **12**, 913-922.
46. E. Eruslanov and S. Kusmartsev, eds., *Identification of ROS Using Oxidized DCFDA and Flow-Cytometry*, Humana Press, London, 2010.
47. H. B. Newton, *Expert. Rev. Neurother.*, 2006, **6**, 1495-1509.
48. J. F. Deeken, *Clin. Cancer Res.*, 2007, 1663-1674.
49. S. B. Tiwari and M. M. Amiji, *Curr. Drug Deliv.*, 2006, **3**, 219-232.
50. R. Alyautdin, I. Khalin, M. I. Nafeeza, M. H. Haron and D. Kuznetsov, *Int. J. Nanomedicine*, 2014, **9**, 795-811.
51. S. R. Hwang and K. Kim, *Arch. Pharm. Res.*, 2014, **37**, 24-30.
52. P. Blasi, S. Giovagnoli, A. Schoubben, M. Ricci and C. Rossi, *Adv. Drug Deliv. Rev.*, 2007, **59**, 454-477.
53. G. Reinhard, *Neurobio. Dis.*, 2009, **37**, 48-57.
54. M. P. Giovanne, *Pharm. Res.*, 1997, **14**, 164-168.
55. S. Wohlfart, S. Gelperina and J. Kreuter, *J. Control. Release.*, 2012, **161**, 264–273.
56. Y. Oh and J. Swanson, *J. Cell. Biol.*, 1996, **132**, 132-585.
57. C. Foged, B. Brodin, S. Frokjaer and A. Sundblad, *Int. J. Pharm.*, 2005, **298**, 315–322.
58. H. Hillaireau and P. Couvreur, *Cell Mol. Life Sci. CMLS.*, 2009, **66**, 2873-2896.
59. P. R. Lockman, *Drug Dev. Ind. Pharm.*, 2002, **28**, 1-13.
60. M. Malakoutikhah, M. Teixido and E. Giralt, *Angew. Chem. Int. Ed. Engl.*, 2011, **50**, 7998-8014.
61. I. van Rooy, E. Mastrobattista, G. Storm, W. E. Hennink and R. M. Schiffelers, *J. Control. Release.*, 2011, **150**, 30-36.
62. C. M. Bergamini, S. Gambetti, A. Dondi and C. Cervellati, *Curr. Pharm. Design.*, 2004, **10**, 1611-1626.
63. B. Halliwell and J. M. C. Gutteridge, *Free Radicals in Biology and Medicine*, Oxford University Press, 2007.
64. M. F. Rivelilson, M. M. V. Silvânia, C. F. S. Francisca, S. B. V. Glauce and M. F. F. Marta, *FEBS J.*, 2005, **272**, 1307–1312.
65. H. Daniel and W. G. M. B. Hendrikus, *Trends Pharmacol. Sci.*, 1993, **14**, 270–275.
66. T. Kishido, K. Unno, H. Yoshida, D. Choba, R. Fukutomi, S. Asahina, K. Iguchi, N. Oku and M. Hoshino, *Biogerontology*, 2007, **8**, 423-430.
67. D. Drescher, G. Orts-Gil, G. Laube, K. Natte, R. W. Veh, W. Osterle and J. Kneipp, *Anal. Bioanal. Chem.*, 2011, **400**, 1367-1373.
68. T. Xia, M. Kovochich, J. Brant, M. Hotze, J. Sempf, T. Oberley, C. Sioutas, J. I. Yeh, M. R. Wiesner and A. E. Nel, *Nano Lett.*, 2006, **6**, 1794-1807.
69. H. Meng, T. Xia, S. George and A. E. Nel, *ACS Nano*, 2009, **3**, 1620-1627.
70. J. Shi, H. L. Karlsson, K. Johansson, V. Gogvadze, L. Xiao, J. Li, T. Burks, A. Garcia-Bennett, A. Uheida, M. Muhammed, S. Mathur, R. Morgenstern, V. E. Kagan and B. Fadeel, *ACS Nano*, 2012, **6**, 1925-1938.
71. S. J. Soenen, W. J. Parak, J. Rejman and B. Manshian, *Chem. Rev.*, 2015, **115**, 2109-2135.
72. V. Stone, H. Johnston and M. J. Clift, *IEEE. T. NanoBiosci.*, 2007, **6**, 331-340.
73. A. A. Shvedova, E. Kisin, A. R. Murray, V. J. Johnson, O. Gorelik, S. Arepalli, A. F. Hubbs, R. R. Mercer, P. Keohavong and N. Sussman, *Am. J. Physiol.-Lung C.* , 2008, **295**, L552-L565.
74. G. Oberdörster, Z. Sharp, V. Atudorei, A. Elder, R. Gelein, W. Kreyling and C. Cox, *Inhal. Toxicol.*, 2004, **16**, 437-445.
75. L. An, S. Liu, Z. Yang and T. Zhang, *Toxicol. Lett.*, 2012, **213**, 220-227.
76. P. Eun-Jung and P. Kwangsik, *Toxicol. Lett.*, 2009, **184**, 18-25.
77. K. R, R. I, O. TY, V. LA, B. EJ, S. M and P. PN, *Acs Nano*, 2010, **4**, 699-708.
78. S. J. So, I. S. Jang and C. S. Han, *J. Nanosci. Nanotechnol.*, 2008, **8**, 5367-5371.
79. J. Jiang, K. Huo, S, Y. Xin, Y. Xu, Z. Wu, Z. Yu and P. Chu, *Biomaterials*, 2009, **30**, 2661–2665.
80. H. A. Santos, J. Riikonen, J. Salonen, E. Makila, T. Heikkila, T. Laaksonen, L. Peltonen, V. P. Lehto and J. Hirvonen, *Acta Biomater.*, 2010, **6**, 2721-2731.
81. B. Fubini and A. Hubbard, *Free Radical Bio. Med.*, 2003, **34**, 1507–1516.
82. J. A. Imlay and S. Linn, *Science*, 1988, **240**, 1302-1309.
83. B. Halliwell, *Am. J. Med.*, 1991, **91**, 14-22.
84. I. Slowing, C. W. Wu, J. L. Vivero-Escoto and V. S. Lin, *Small*, 2009, **5**, 57-62.
85. A. Holmgren, *Biochem. Soc. Transact.*, 2005, **33**, 13963-13966.
86. M. B. Toledano, C. Kumar, N. Le Moan, D. Spector and F. Tacnet, *FEBS letters*, 2007, **581**, 3598-3607.
87. C. Sayes, M., A. M. Gobin, K. D. Ausman, J. Mendez, J. L. West and V. L. Colvin, *Biomaterials*, 2005, **26**, 7587-7595.
88. S. H. Graham and J. Chen, *J. Cerebr. Blood. F. Met.* , 2001, **21**, 99-109.
89. J. C. Reed, *J. Cell Biol.*, 1994, **124**, 1-6.
90. J. C. Reed, J. M. Jurgensmeier and S. Matsuyama, *Biochimica. Et. Biophysica. Acta*, 1998, **1366**, 127–137.

Table of content entry

FOR

Implication for blood-brain-barrier permeability, *in vitro* oxidative stress and neurotoxicity potential induced by mesoporous silica nanoparticles: effects of surface modification

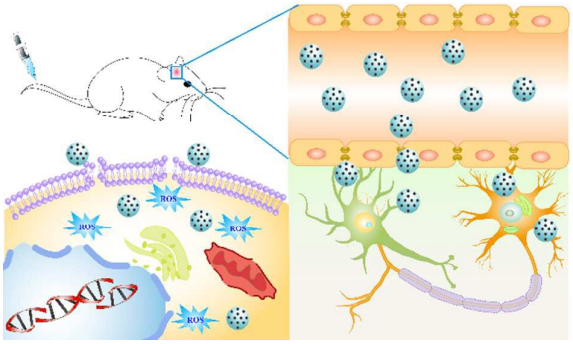

The MSNs show the potential to overcome the BBB and cause neuronal damage, however, neurotoxicity potential could be mediated with surface modification.